

Random walk on the Bloch sphere realized by a simultaneous feedback and feed-forward control in a superconducting Xmon qubit system

Liang Xiang,¹ Zhiwen Zong,¹ Zhenhai Sun,¹ Ze Zhan,¹ Ying Fei,¹ Zhangjingzi Dong,¹ Chongxin Run,¹ Zhilong Jia,² Peng Duan,² Jianlan Wu,^{1,*} Yi Yin,^{1,†} and Guoping Guo^{2,3,‡}

¹*Zhejiang Province Key Laboratory of Quantum Technology and Device,
Department of Physics, Zhejiang University, Hangzhou, 310027, China*

²*Key Laboratory of Quantum Information,
University of Science and Technology of China, Hefei, 230026, China*

³*Origin Quantum Computing, Hefei, 230026, China*

Abstract

Measurement-based feedback control is central in quantum computing and precise quantum control. Here we realize a fast and flexible field-programmable-gate-array-based feedback control in a superconducting Xmon qubit system. The latency of room-temperature electronics is custom optimized to be as short as 140 ns. Projective measurement of a signal qubit produces a feedback tag to actuate a conditional pulse gate to the qubit. In a feed-forward process, the measurement-based feedback tag is brought to a different target qubit for a conditional control. In a two-qubit experiment, the feedback and feed-forward controls are simultaneously actuated in consecutive steps. A quantum number is then generated by the signal qubit, and a random walk of the target qubit is correspondingly triggered and realized on the Bloch sphere. Our experiment provides a conceptually simple and intuitive benchmark for the feedback control in a multi-qubit system. The feedback control can also be further explored to study complex stochastic quantum control.

* jianlanwu@zju.edu.cn

† yiyin@zju.edu.cn

‡ gpguo@ustc.edu.cn

I. INTRODUCTION

Quantum feedback is an important element to realize fault-tolerant quantum computation in a complex multi-qubit system [1]. Quantum feedback is defined as a conditional action back to the quantum system, based on the results of quantum state measurement of qubits in the original system [2, 3]. Quantum error correction depends on repeated measurements of qubit states and the feedback control to correct the error in a redundant quantum system [1]. The superconducting qubit system is a promising platform to develop the quantum feedback and quantum error correction [4]. Although an autonomous or coherent feedback can be realized without any external logical decision hardware [5–7], the measurement-based feedback control is a natural choice to provide feedback to the quantum system [8–17], with the controller itself a classical instrument.

In different measurement-based feedback control protocols, both analog feedback and digital feedback systems have been developed [8–17]. The analog feedback is often based on partial measurements and acts to the qubit with continuous parameter [8, 13]. The digital feedback based on projective measurement is very flexible and can be directly applied to multi-qubit protocols. A relative fast digital feedback control [15–17] is promising for the future complex applications [18–21]. Here we realize a fast electronic feedback control system in a multi-qubit framework, based on a customized field-programmable-gate-array (FPGA) setup. The latency of room-temperature electronics has been optimized to be as short as 140 ns. Although in our current status the delay of feedback loop is mainly limited by the relative long measurement pulse, the short latency of electronics will speed up the whole process when a Purcell filter is included for a fast measurement [4, 22, 23].

Different benchmarks of the feedback control have been designed and presented previously [8, 9, 11, 12, 17]. The feedback control in our system is all based on a high-fidelity projective measurement of the superconducting qubit. The function of feedback is initially proved by a reset experiment, in which a single qubit is reset to the ground state with a feedback-reset-gate [9]. The qubit is further frozen by the feedback to an arbitrary state on the Bloch sphere [12], with the superposition state $(|0\rangle + |1\rangle)/\sqrt{2}$ as an example. For both single-qubit experiments, the feedback control can be applied consecutively for multiple times, which enables a high-fidelity qubit reset and a repeated frozen state.

The feedback control in a multi-qubit system is often applied to measure the parity of

entangled qubits to create tag for following conditional gates [10, 17]. The corresponding concepts are relatively complicated from the engineering point of view. Here we bring a simple and intuitive experiment to benchmark the feedback control in a multi-qubit system. We choose a signal qubit and a target qubit for two-qubit experiments. The signal qubit is measured to produce a tag for the feedback control. If the tag is sent to bring a conditional gate to the signal qubit itself, the feedback control is similar as that in the single-qubit experiments. If the tag is sent to bring a conditional gate to the target qubit, this feedback control is named a feed-forward process. When the feedback and feed-forward controls simultaneously take effect, specified functions can be realized.

A random walk is a stochastic or random process by which an object wanders away from its starting position. The random walk depends on random number generators to take successive random steps on a one-dimensional (1D), two-dimensional (2D) or even higher dimensional parameter space. In practice, most engineered random walk processes apply computer-generated pseudo-random numbers, a deterministic sequence expanded from a seed. We prepare the signal qubit at the superposition state $(|0\rangle + |1\rangle)/\sqrt{2}$ and create a tag based on the projective measurement. In this way, the signal qubit can function as a random number generator (0 or 1) for controlled manipulation of the target qubit. Here the target qubit is actuated to rotate clockwise or anticlockwise with a designated angle. When the signal qubit is repeatedly frozen at $(|0\rangle + |1\rangle)/\sqrt{2}$ and generate the random number for multiple steps, the target qubit can be actuated by the simultaneous feed-forward control to realize a random walk on the Bloch sphere. We present measured results for a random walk with one step, two steps and three steps. When the precise control of qubits is improved later, more complex random walk can be realized by the feedback control, such as a random walk with more steps or even a 2D random walk on the Bloch sphere. This scheme of feedback control in a multi-qubit system can be directly applied in the quantum error correction.

II. EXPERIMENTAL SYSTEM INCLUDING THE FEEDBACK CONTROL

A schematic diagram of our experimental setup is shown in Fig. 1(a). A superconducting Xmon qubit chip is mounted in a dilution refrigerator (DR) at a base temperature of 10 mK. Through some cryogenic filters and amplifiers, input and output lines of the qubit system are connected to corresponding room-temperature electronics. We mainly list three FPGA-

based boards, which are key elements in the feedback loop to measure, control and provide feedback signal to the superconducting qubit system.

Two Xmon qubits Q_A and Q_B are utilized in the following feedback experiment. They are physically separated by three qubits in a linear array of capacitively-coupled qubits, with the similar qubit and chip described before [24–26]. Two Xmon qubits are both biased at the sweet point [27] with a fixed operation frequency of $\omega_{qA}/2\pi = 5.050$ GHz and $\omega_{qB}/2\pi = 5.079$ GHz, respectively. The energy relaxation time T_1 are $16 \mu\text{s}$ and $19 \mu\text{s}$, and the pure decoherence time T_2^* are $20 \mu\text{s}$ and $33 \mu\text{s}$ for Q_A and Q_B , respectively. The qubit state is readout by a dispersive method through a coupled readout resonator. The resonator bare frequencies are $\omega_{rA}/2\pi = 6.521$ GHz and $\omega_{rB}/2\pi = 6.438$ GHz for Q_A and Q_B , respectively. In the dispersive readout, a shaped readout pulse is sent through the readout line, and encode a qubit-state-dependent dispersive shift of the readout resonator. The readout signal is then amplified by a low-temperature Josephson parametric amplifier (JPA) [28] and a high electron mobility transistor (HEMT). The amplified signal finally goes into room temperature electronics for a data collection and analysis.

The first FPGA board (BD1) is specially designed for the function of qubit-state readout. With the FPGA algorithm, two digital-to-analog-converter (DAC) output shaped pulses with a carrier frequency smaller than the DAC Nyquist frequency of 500 MHz. They are sent out to an IQ mixer as two quadratures, $I(t)$ and $Q(t)$. A microwave source provides a local oscillator (LO) signal ($f = 6.475$ GHz) for the IQ mixer, which is modulated by the IQ quadratures to generate a readout signal with variable frequency, phase and amplitude [4]. For the detection of returned signal, another IQ mixer mixes down the signal to two IQ quadratures, which are further digitized by two analog-to-digital-converter (ADC) in BD1. With a demodulation processing, the readout result is represented as data points in a two-dimensional plane spanned by I and Q .

In our experiment, the readout pulse has a quick initial overshoot and a following sustain part [23, 29]. The pulse amplitude is optimized for a projective measurement, in which the qubit is projected to the ground $|0\rangle$ or excited $|1\rangle$ state with probabilities determined by the final qubit state before measurement. With a 800 ns long readout pulse and a repetition of the same measurement for many times ($C_{\text{tot}} = 1 \times 10^4$), a typical distribution of readout result for Q_B is shown in the IQ plane in Fig. 1(b). The blue and red dots represent result for the ground $|0\rangle$ and excited $|1\rangle$ state, respectively. They are observed to be two separated

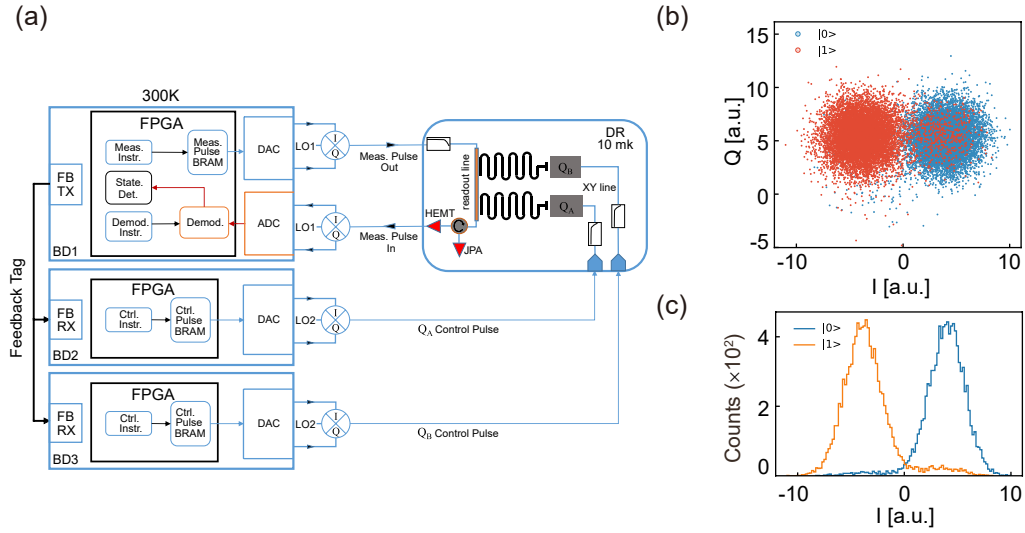


FIG. 1. (a) Schematic diagram of the experimental system. Three customized FPGA-based boards are main control electronics of the feedback loop. The board BD1 contains 1 FPGA mother board and 2 DAC/ADC daughter cards. The FPGA mother board reads experimental instructions, fetches the measure pulse preloaded at the block random access memory (BRAM), and streams it to the DAC card. The measure pulse at base-band (< 500 MHz) is up-converted to the carrier frequency using an analog IQ mixer and a microwave signal (LO1). Another IQ mixer down-converts the returned measure pulse to the base-band, and the ADC card digitize the IQ signals. The digital IQ signals are further processed by the demodulation logic and state determination logic. The feedback transmit (TX) logic encapsulates the measurement result (0 or 1) to create a feedback tag, which is broadcasted to other boards. The boards BD2 and BD3 receive the feedback tag and accordingly generate the conditional qubit control pulse. (b) With Q_B initialized in the ground state $|0\rangle$ (blue) or excited state $|1\rangle$ (red), the measured results are displayed in the IQ plane with blue or red points, respectively. (c) Statistical histogram of (b) on the I axis, after data points integrated with respect to the Q axis.

humps of data points with a Gaussian distribution. The centers of two Gaussian humps are connected and intentionally rotated to be horizontal in the IQ plane, by adjusting the initial phase of the readout pulse. A line symmetrically intersecting the connection line can be chosen as a threshold to separate the qubit state. The threshold I value has been shifted to 0 in the shown figure.

The number of data points is integrated with respect to the Q axis and the histogram of I is shown in Fig. 1(c). For the ground state $|0\rangle$, the main Gaussian hump is on the right side with I larger than 0. For the excited state $|1\rangle$, the main Gaussian hump is on the left side with I smaller than 0. For both $|0\rangle$ and $|1\rangle$, there are still scattered data points on the other side of the threshold line. The readout fidelity of the ground (excited) state is defined as the fraction of counted points with I larger (smaller) than 0 over C_{tot} , leading to $F_{\text{qB}}^0 \approx 97.3\%$ and $F_{\text{qB}}^1 \approx 90.3\%$ in Fig. 1c. For the other qubit Q_A , the two readout fidelities are $F_{\text{qA}}^0 \approx 96.1\%$ and $F_{\text{qA}}^1 \approx 93.1\%$. The readout fidelity for the excited state is normally smaller than that for the ground state, mainly due to the qubit decay error in the measurement process.

The BD1 board enables a multiplexed dispersive readout, in which readout pulses at different frequencies can be multiplexed in the same readout line. The readout signal is finally demodulated to different channels, giving the qubit state result for each individual qubit. In the current version, the FPGA algorithm in BD1 admits a simultaneous measurement of eight qubits.

In the feedback control, a signal qubit is chosen to provide a feedback tag for the superconducting qubit system. By comparing each measured I with the threshold value, the qubit state of the signal qubit is determined to be at the ground or excited state. Correspondingly a feedback tag can be generated and transferred from the feedback transmit (TX) to the receive (RX) channels of other FPGA boards. After receiving a feedback tag, the other FPGA boards (BD2 and BD3) can output a conditional shaped pulse. The DAC output is up-converted by the IQ mixer and another microwave source (LO2 with $f = 4.800$ GHz) to the qubit transition frequency. The different feedback-tag-controlled pulses are transferred through XY control lines to the corresponding qubits to implement a conditional quantum gate. For example, if Q_A is designated as the signal qubit, the feedback-tag-controlled output of BD2 is a feedback control on Q_A , and the similar output of BD3 is a feed-forward control on Q_B . The DAC output of BD2 and BD3 also provide pulses for general qubit operations of Q_A and Q_B , respectively. This scheme can be extended to a superconducting system with many qubits, and multiple signal qubits can be chosen for the feedback control in each subgroup of qubits.

The three boards and the microwave source are phase-locked to an external 10 MHz clock. The timing between different boards are synchronised, with the time dependent pulse

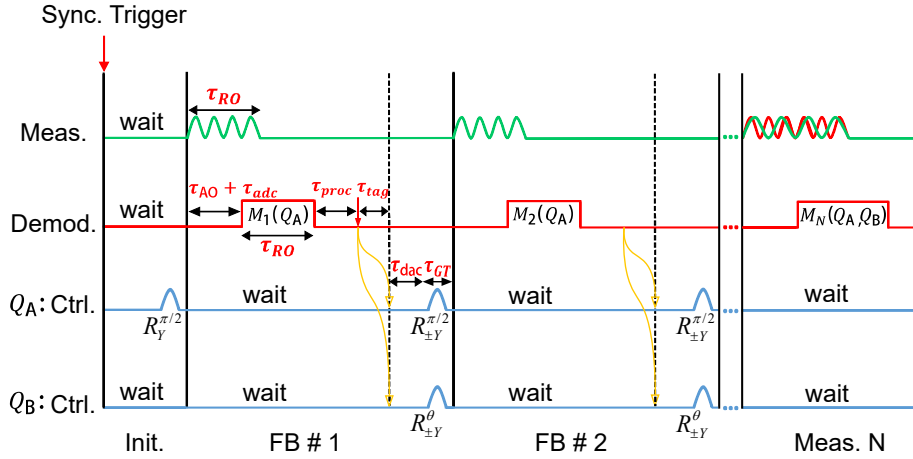


FIG. 2. Schematic diagram of the pulse sequence. From top to bottom are readout pulses, demodulation windows and control pulses of the signal qubit Q_A and the target qubit Q_B . The sequence is synchronized by a trigger signal.

sequence shown in the schematic diagram in Fig. 2. The feedback latency in the feedback loop can be correspondingly determined. In all related time scales, τ_{RO} is the readout pulse length and τ_{GT} is the pulse length of the conditional gate. These two scales are variable parameters in the feedback loop. Starting from the readout pulse, there is a total delay in the low-temperature analog devices and cables, τ_{AO} , before the signal returns to the ADC. The latency τ_{adc} is introduced by the ADC, which is about 16 ns. The demodulation processing takes a delay of $\tau_{proc} = 32$ ns, determined by the clock period (4 ns) and number of Flip-Flops used in the FPGA fabric. The latency τ_{tag} is measured to be 24 ns on the oscilloscope. After receiving the feedback tag, there is another delay τ_{dac} (68 ns) before the conditional gate pulse is sent out. We define a total delay for the room temperature electronics, $\tau_{tot} = \tau_{adc} + \tau_{proc} + \tau_{tag} + \tau_{dac}$, which is 140 ns in the current status. The optimized τ_{tot} enables a fast feedback control in our setup.

III. RESULTS

The feedback control is first applied to reset a qubit to the ground state $|0\rangle$, which can simply prove the realization of a feedback function [9]. The Xmon qubit Q_A is utilized for

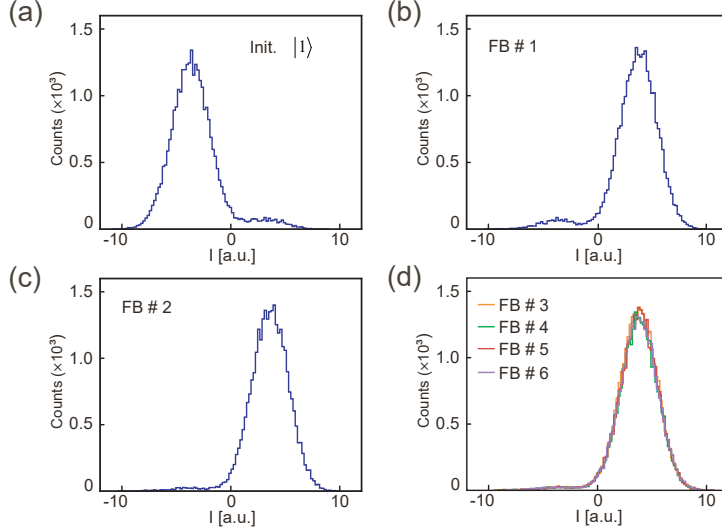


FIG. 3. (a) The histogram of I signal for qubit Q_A initialized at the excited state $|1\rangle$. (b) The histogram of I signal when qubit Q_A is reset to the ground state $|0\rangle$ by a feedback control. (c) The histogram of I signal when qubit Q_A is further reset to $|0\rangle$ by the 2nd feedback control. (d) The histogram of I signal when qubit Q_A is consecutively reset to $|0\rangle$ by multiple feedback controls.

this single-qubit experiment. The idle qubit is initially prepared at the excited state $|1\rangle$ with a calibrated π pulse. Afterwards a feedback-reset-gate is applied, which includes a dispersive qubit state measurement and a conditional control pulse. If the qubit is measured to be at the excited state, the conditional control is designated as a π pulse to reset the qubit to the ground state. If the qubit is measured to be at the ground state, the control gate is instead designated as an empty sequence but waiting for the same time as the duration of the π pulse. Afterwards the qubit is measured again to check the effectiveness of the feedback-reset-gate. The same procedure has been repeated for $C_{\text{tot}} = 3 \times 10^4$ times. We integrate the number of data points with respect to the Q axis and show the histograms of I in Fig. 3. In Fig. 3(a), The main distribution of data points shows a hump with Gaussian distribution on the left side, with I smaller than 0. The calculated ratio of the excited-state probability is 93.0%. For the qubit-state measurement after the conditional feedback control, most of the data points in Fig. 3(b) concentrate on the right side, also showing a hump with Gaussian distribution. The main distribution of qubit state shifts from the left side to the right side means that the initialized qubit (at excited state $|1\rangle$) is reset to the ground state $|0\rangle$, by the conditional feedback control. In Fig. 3(b), a small hump can also be observed on the left side

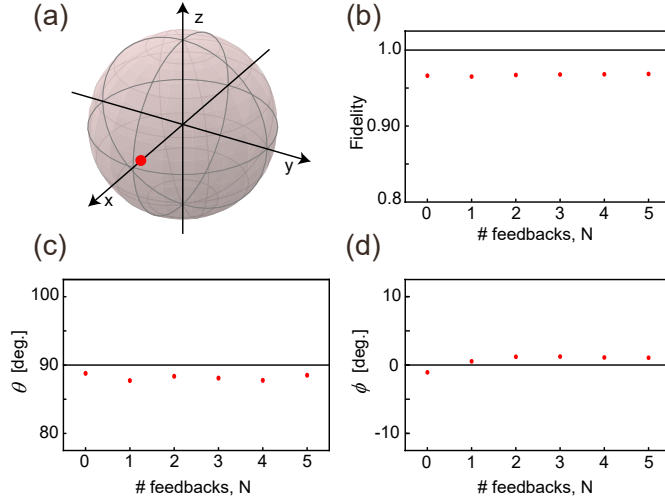


FIG. 4. (a) After initialized at the superposition state $(|0\rangle + |1\rangle)/\sqrt{2}$, the qubit Q_A is measured with a quantum state tomography (QST), with the measured Bloch vector displayed as a single point on the Bloch sphere. (b) With qubit Q_A consecutively frozen at the superposition state $(|0\rangle + |1\rangle)/\sqrt{2}$ by multiple feedback controls, the qubit state are measured by the QST and the state fidelity are correspondingly calculated and displayed. (c) From the QST measurements, the polar angle θ of the Bloch vector are extracted and displayed. (d) The azimuth angle ϕ of the Bloch vector are extracted and displayed.

with a probability of 6.3%. One source of error can be attributed to the qubit state decay between the 1st measurement and the conditional pulse, in which the conditional π pulse rotates the decayed qubit to the excited state again. The feedback function can be enabled consecutively for multiple times [16, 17, 30]. After the 2nd measurement, we apply another conditional gate based on the measurement result. Then a 3rd measurement is taken to check the result, with the histogram of I shown in Fig. 3(c). Compared with Fig. 3(b), Fig. 3(c) shows a similar distribution, but with the small hump on the left side depressed to a probability of 3.5%. The similar feedback control has been repeated for six times, with the multiple measurements shown in Fig. 3(d). The consecutive feedback controls lead to a steady state, with a fidelity of 96.5% for the reset ground state.

Reset the qubit to the ground state is a special application of the feedback control. Because of the flexibility of the conditional gate, the feedback control can be applied to freeze the qubit to any quantum state on the Bloch sphere [12]. The superposition state

$(|0\rangle + |1\rangle)/\sqrt{2}$ is taken as an example. The qubit is initialized at $\Psi = (|0\rangle + |1\rangle)/\sqrt{2}$ by a $\pi/2$ rotation around the y axis. Then the qubit is measured with a projective measurement. If the qubit is projected to the ground (excited) state, a conditional $\pi/2$ pulse around the y ($-y$) axis encoded in the algorithm is applied in the feedback control. No matter what the intermediate measurement result is, the qubit is brought back to the state $(|0\rangle + |1\rangle)/\sqrt{2}$. A quantum state tomography (QST) is applied to measure the frozen state (see Appendix A) [1, 31]. For any qubit state, a density matrix can be expanded as $\rho = 1/2(\mathbf{I} + \mathbf{r} \cdot \boldsymbol{\sigma})$, where \mathbf{I} and $\boldsymbol{\sigma}$ are the identity and pauli matrices. Determined with the QST measurement, the Bloch vector $\mathbf{r} = (x, y, z)$ can be depicted as a single point on the Bloch sphere. As shown in Fig. 4(a), the Bloch vector of the frozen state is plotted, which points to the x axis and is consistent with the expected state of $(|0\rangle + |1\rangle)/\sqrt{2}$. The fidelity of the frozen state $F = \langle \Psi | \rho | \Psi \rangle$ is calculated to be 96.6%. Similar to the reset experiment, the qubit state can be frozen to the designated state by consecutive feedback controls. All the intermediate qubit-state readout is a projective measurement. After a finite times of conditional feedback controls, the final qubit state is measured with a QST. For the consecutive frozen states, θ and ϕ of the Bloch vector \mathbf{r} are displayed in Fig. 4(c) and 4(d), respectively. The error of θ is all smaller than 2.5° and the error of ϕ is all smaller than 1.5° . As shown in Fig. 4(b), the fidelity of consecutive frozen state is all larger than 96%.

A feedback control applies a conditional gate to a qubit based on the measurement result of the qubit itself. For a multi-qubit system, a feed-forward control can provide special applications in the quantum information processing [10, 11]. To prove the feed-forward function, we choose Q_A as a signal qubit, and Q_B as a target qubit. The feedback tag is generated based on the projective measurement of the signal qubit. Then a feedback-tag-controlled conditional pulse is issued to the target qubit. The two qubits are physically separated by three qubits in the linear array. To ignore any residue interaction, the signal qubit Q_A is biased away from the sweet point, at $\omega_{qA}/2\pi = 4.840$ GHz. The frequency difference between two qubits is increased to $|\omega_{qA} - \omega_{qB}| = 240$ MHz, and two qubits are effectively decoupled from each other. At this operation point of Q_A , the energy relaxation time T_1 is $9.3 \mu\text{s}$ and the pure decoherence time T_2^* is $1.2 \mu\text{s}$.

As a simple example, the signal qubit Q_A is initialized at $(|0\rangle + |1\rangle)/\sqrt{2}$. The projective measurement of the signal qubit is applied for the feed-forward control on the target qubit Q_B , as shown in the schematic diagram in Fig. 5(a). For an ideal state of $(|0\rangle + |1\rangle)/\sqrt{2}$,

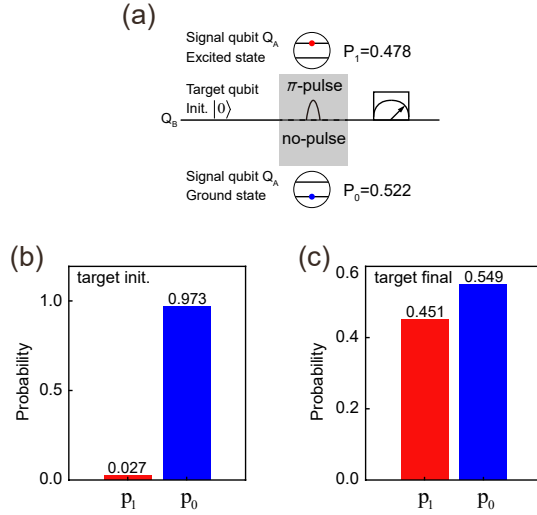


FIG. 5. (a) Schematic diagram showing that the measurement of signal qubit is applied to actuate a conditional pulse gate to the target qubit. With the signal qubit Q_A initialized at the superposition state $(|0\rangle + |1\rangle)/\sqrt{2}$, P_0 (P_1) is the measured probability of Q_A for I larger (smaller) than 0. (b) With the target qubit Q_B initialized at the ground state $|0\rangle$, p_0 (p_1) is the measured probability of Q_B for I larger (smaller) than 0. (c) The measured final probabilities of Q_B after the feed-forward control is applied.

there should be an equal probability of 50% for the qubit to be projected to the state of $|0\rangle$ and $|1\rangle$. Here there is a larger probability of $P_0 = 52.2\%$ for the detection of I signal larger than 0, due to the qubit decay error in the measurement procedure. Correspondingly the probability of I signal smaller than 0 is $P_1 = 47.8\%$ for the initialized Q_A . Note that in the QST measurement, this decay effect is weakened because the z -projection is averaged from the results under the operations of an identity and a $U_y(\pi)$ gate (Appendix A). For the target qubit Q_B , it is initialized at the ground state $|0\rangle$, with a measured histogram shown in the bottom left panel in Fig. 5(b). For simplicity, we integrate the number of data points in the IQ plane for I both smaller and larger than zero, and show two ratio bars for the ground and excited state probabilities. The probability of I larger than 0 is 97.3% for the initialized target qubit Q_B . For the feed-forward control, a π (empty) pulse is applied to Q_B if Q_A is measured to be at the excited (ground) state. Afterwards the qubit state of Q_B is measured for checking the function of the feed-forward control. From an ensemble measurement of the target qubit Q_B , its state probability is determined as

shown in the histogram in Fig. 5(c). With the signal qubit in the state of $(|0\rangle + |1\rangle)/\sqrt{2}$, there is approximately a 50% probability for the qubit to be pumped to the excited state. With a relative smaller ratio ($P_1 = 47.8\%$) for Q_A to be in the excited state, there is also a relative smaller ratio for Q_B to be pumped to the excited state. The probability for Q_B to be at $|0\rangle$ ($|1\rangle$) can be statistically simulated by $p_f^0 = p_0P_0 + p_1P_1$ ($p_f^1 = p_0P_1 + p_1P_0$), where P_0/P_1 and p_0/p_1 are the initialized probabilities of Q_A and Q_B , respectively. The simulation result is $p_f^0 = 52.1\%$ and $p_f^1 = 47.9\%$. After a measurement correction (Appendix A), the simulation result can be calibrated to $p_f^0 = 55.3\%$ and $p_f^1 = 44.7\%$, well consistent with the experimental result.

For the random walk experiment, qubit Q_A is utilized as a signal qubit and prepared at $(|0\rangle + |1\rangle)/\sqrt{2}$. The projective measurement of this qubit produces a quantum random number of 0 or 1, and a corresponding feedback tag to control the target qubit. The target qubit Q_B is initially prepared at the ground state $|0\rangle$ (the north pole in the Bloch sphere). Depending on the 1st measurement of the signal qubit, the feedback control is a conditional pulse to rotate the target qubit away from the north pole. For the signal qubit measured in the ground or excited state, we rotate Q_B around the y -axis or $-y$ -axis with angle θ , respectively. After the operation of R_y^θ or R_{-y}^θ , a collection of tomography pulses are further applied for the QST measurement of Q_B . Because we can record each measurement result of the signal qubit, the measurement for the target qubit with R_y^θ and R_{-y}^θ rotations can be separately collected for the QST measurement. For an example of $\theta = \pi/8$, the tomography result for the one-step random walk is shown in the Bloch sphere in Fig. 6(a). Looking at the xz -plane from the $-y$ -axis, the state vector is observed to rotate to the right or left side of the north pole. In the right panel of Fig. 6(a), we show both measured angles of the state vector in the QST. To distinguish the two random-walk directions, the clockwise rotation is labeled with a positive angle while the anticlockwise rotation is labeled with a negative angle. The measured angles slightly deviate from the ideal value with an error of -0.32° and 0.36° for signal qubit at $|0\rangle$ and $|1\rangle$, respectively. The percentage of the collected data in QST is also shown for the two vectors. There is a relative larger ratio (52.9%) for the target qubit to rotate clockwise, due to the qubit-decay-induced larger ratio for signal qubit at $|0\rangle$. The background grey bars are centered at ideal angles, while the height of each grey bar is set to the corresponding experimental result.

To apply consecutive feed-forward controls for the multi-step random walk on the Bloch

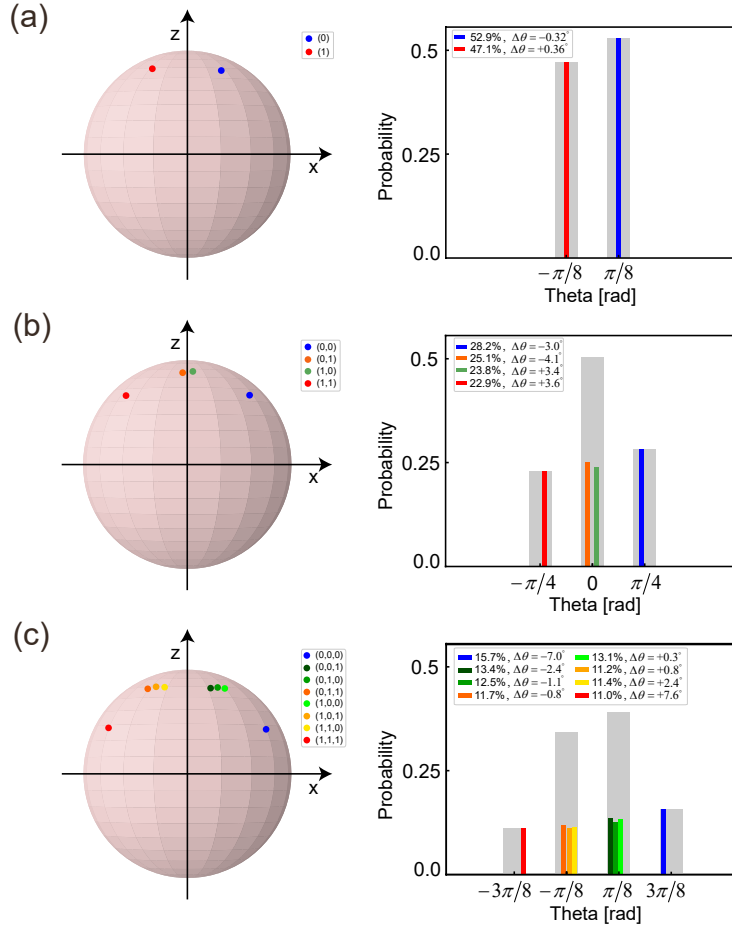


FIG. 6. (a) QST result of the one-step random walk of the target qubit, which is drawn as data points of state vectors on the xz -plane of the bloch-sphere. In the right panel, the polar angles of clockwise and anticlockwise rotations of the random walk are shown by the blue and red bars, respectively. The grey bars are centered at ideal angles. The height of both colored bars and grey bars is the percentage of collected data in corresponding QST measurement. (b) QST result of the two-step random walk of the target qubit. (c) QST result of the three-step random walk of the target qubit.

sphere, the signal qubit is simultaneously frozen at $(|0\rangle + |1\rangle)/\sqrt{2}$ by a feedback control at each step. After the 1st measurement of the signal qubit, the target qubit is rotated clockwise or anticlockwise, with an angle of $\theta = \pi/8$ or $\theta = -\pi/8$. After the 2nd measurement of the signal qubit, the target qubit is assigned to rotate again depending on the feedback tag, no matter how the 1st-step rotation evolves. The target qubit is then appended with

tomography pulses for the final-state determination. Here the feedback measurement can be collected to four groups $\{00, 01, 10, 11\}$, with the two numbers representing the 1st and 2nd measurement results of the signal qubit. For each group of ensemble measurement, the tomography result is collected for extracting the final state on the Bloch sphere, as shown in Fig. 6(b). If a reversed walk is involved, the qubit is rotated back to be close to the north pole, as shown for the two vectors related with $\{01\}$ and $\{10\}$. In the right panel of Fig. 6(b), we present measured angles of state vectors and corresponding percentages of collected data for the two-step random walk. For signal qubit at state of $\{00\}$ and $\{11\}$, the measured angles deviate from the ideal value with an error of -3.0° and 3.6° , respectively. For groups of $\{01\}$ and $\{10\}$, a small difference happens between the percentages of two vectors, due to the slight variation of probabilities for consecutive frozen state of the signal qubit. The height of the central grey bar is set to the addition of two percentages. A three-step random walk is similarly actuated by the simultaneous feedback and feed-forward control, with the results shown in Fig. 6(c). For groups of $\{000\}$ and $\{111\}$, the measured angles deviate from ideal values with an error of -7.0° and 7.6° , respectively. Compared with angles related with $\{00\}$ and $\{11\}$ in the two-step random walk, and angles related with $\{0\}$ and $\{1\}$ in the one-step random walk, the angle error increases with the number of walk steps, which is found to be related with the qubit-decay in the simulation analysis. For groups of $\{001\}$, $\{010\}$ and $\{101\}$, state vectors share similar vector angles around $\theta = \pi/8$, and the height of the grey bar is set to the addition of three percentages. The similar behavior happens for groups of $\{011\}$ and $\{110\}$. The measured random walk of target qubit on the Bloch sphere proves both the realization of consecutive feedback/feed-forward control and the precise quantum control in our superconducting multi-qubit system.

IV. SUMMARY

We develop a fast FPGA-based feedback control system, with the latency of room-temperature electronics optimized to 140 ns. The function of feedback control is proved by resetting the qubit to the ground state and freezing the qubit to a designated superposition state with high-fidelity. In two-qubit experiments, projective measurement of the signal qubit provides a feed-forward control to the target qubit. The consecutive and simultaneous feedback and feed-forward control enables a random walk of the target qubit on the

Bloch sphere. Our experiment is a conceptually simple benchmark for the feedback control in a multi-qubit system. The random walk experiment can be explored further to study the quantum number generator and stochastic quantum control. For example, the current conditional random walk depends on the present measurement of the signal qubit, which is a memoryless Markov process. By modifying the binary tree to a quadtree in the feedback control, the random walk can be extended to depend on both the present and the previous measurement of the signal qubit (a non-Markovian process with memory).

ACKNOWLEDGMENTS

The work reported here was supported by the National Basic Research Program of China (Grants No. 2015CB921004), the National Key Research and Development Program of China (Grant No. 2016YFA0301700), the National Natural Science Foundation of China (Grants No. 11775129, No. 11575101 and No. 11934010) and the Anhui Initiative in Quantum Information Technologies (Grant No. AHY080000). Y.Y. acknowledge the funding support from Tencent Corporation. This work was partially conducted at the University of Science and Technology of the China Center for Micro- and Nanoscale Research and Fabrication.

Appendix A: Quantum State Tomography (QST) Measurement

To fully determine the quantum state of a two-level qubit, we need to realize the quantum state tomography (QST) measurement. The density matrix of either a pure or mixed state can be expanded as $\rho = \frac{1}{2} (I + x\sigma_x + y\sigma_y + z\sigma_z)$, with $I = |0\rangle\langle 0| + |1\rangle\langle 1|$. We introduce three Pauli operators, $\sigma_x = |0\rangle\langle 1| + |1\rangle\langle 0|$, $\sigma_y = -i|0\rangle\langle 1| + i|1\rangle\langle 0|$, and $\sigma_z = |0\rangle\langle 0| - |1\rangle\langle 1|$, based on which a vector of Pauli operators is represented by $\boldsymbol{\sigma} = (\sigma_x, \sigma_y, \sigma_z)$. The three projections, x , y and z along the three directions, determine a vector, $\boldsymbol{r} = (x, y, z)$, which is named as the Bloch vector. The z -projection, $z = P_0 - P_1$, is extracted from a projective measurement of the qubit probability. To extract the x -projection, we rotate the quantum state by an angle of $-\pi/2$ around the y -axis and the density matrix is changed to be $\rho' = U_y(-\pi/2)\rho U_y^\dagger(-\pi/2)$, where $U_\zeta(\theta) = \exp[-i\theta\sigma_\zeta/2]$ is an unitary operator for a rotation angle of θ around the $\zeta(= x, y, z)$ -axis. Experimentally, the $U_\zeta(\theta)$ gate is realized by a calibrated pulse with the

frequency ω_{10} . The rotated density matrix is then given by $\rho' = (I_2 - z\sigma_x + y\sigma_y + x\sigma_z)/2$. The population measurement determines the x -projection, $x = P'_0 - P'_1$, where P'_0 and P'_1 are the populations of the ground and excited states in the rotated density matrix. In practice, the $U_y(\pi/2)$ gate is also applied for the measurement and the x -projection is averaged from the results under the operations of the $U_y(\pi/2)$ and $U_y(-\pi/2)$ gates. The y -projection is similarly obtained using the operations of the $U_x(\pi/2)$ and $U_x(-\pi/2)$ gates.

Appendix B: Measurement Correction

From the readout fidelity measured for both ground (F_0) and excited (F_1) state, we could observe that the measured population probabilities (P^m) are often different from the ideal result (P^i). The relation between the ideal and measured populations can be expressed as

$$\begin{pmatrix} P_0^m \\ P_1^m \end{pmatrix} = \begin{pmatrix} F_0 & 1 - F_1 \\ 1 - F_0 & F_1 \end{pmatrix} \begin{pmatrix} P_0^i \\ P_1^i \end{pmatrix}, \quad (\text{B1})$$

from which the ideal populations can be calibrated from measured population probabilities.

-
- [1] M. A. Nielsen, I. Chuang and L.K.Grover, Quantum Computation and Quantum Information, Cambridge University Press, Cambridge, England, 2010.
 - [2] M. Sarovar, H. S. Goan, T. P. Spiller, and G. J. Milburn, High-Fidelity Measurement and Quantum Feedback Control in Circuit QED, Phys. Rev. A. 72, 062327 (2005).
 - [3] N. Yamamoto, Coherent Versus Measurement Feedback: Linear Systems Theory for Quantum Information, Phys. Rev. X 4, 041029 (2014).
 - [4] P. Krantz, M. Kjaergaard, F. Yan, T. P. Orlando, S. Gustavsson, and W. D. Oliver, A Quantum Engineer's Guide to Superconducting Qubits, Appl. Phys. Rev. 6, 021318 (2019).
 - [5] K. Geerlings, Z. Leghtas, I. M. Pop, S. Shankar, L. Frunzio, R. J. Schoelkopf, M. Mirrahimi, and M. H. Devoret, Demonstrating a Driven Reset Protocol for a Superconducting Qubit, Phys. Rev. Lett. 110, 120501 (2013).
 - [6] S. Shankar, M. Hatridge, Z. Leghtas, K. M. Sliwa, A. Narla, U. Vool, S. M. Girvin, L. Frunzio, M. Mirrahimi, and M. H. Devoret, Autonomously Stabilized Entanglement between Two Superconducting Quantum Bits, Nature 504, 419 (2013).

- [7] Y. Liu, S. Shankar, N. Ofek, M. Hatridge, A. Narla, K. M. Sliwa, L. Frunzio, R. J. Schoelkopf, and M. H. Devoret, Comparing and Combining Measurement-Based and Driven-Dissipative Entanglement Stabilization, *Phys. Rev. X* 6, 011022 (2016).
- [8] R. Vijay, C. Macklin, D. H. Slichter, S. J. Weber, K. W. Murch, R. Naik, A. N. Korotkov, and I. Siddiqi, Stabilizing Rabi Oscillations in a Superconducting Qubit Using Quantum Feedback, *Nature* 490, 77 (2012).
- [9] D. Risté, C. C. Bultink, K. W. Lehnert, and L. Dicarlo, Feedback Control of a Solid-State Qubit Using High-Fidelity Projective Measurement, *Phys. Rev. Lett.* 109, 240502 (2012).
- [10] D. Risté, M. Dukalski, C. A. Watson, G. De Lange, M. J. Tiggelman, Y. M. Blanter, K. W. Lehnert, R. N. Schouten, and L. Dicarlo, Deterministic Entanglement of Superconducting Qubits by Parity Measurement and Feedback, *Nature* 502, 350 (2013).
- [11] L. Steffen, Y. Salathe, M. Oppliger, P. Kurpiers, M. Baur, C. Lang, C. Eichler, G. Puebla-Hellmann, A. Fedorov, and A. Wallraff, Deterministic Quantum Teleportation with Feed-Forward in a Solid State System, *Nature* 500, 319 (2013).
- [12] P. Campagne-Ibarcq, E. Flurin, N. Roch, D. Darson, P. Morfin, M. Mirrahimi, M. H. Devoret, F. Mallet, and B. Huard, Persistent Control of a Superconducting Qubit by Stroboscopic Measurement Feedback, *Phys. Rev. X* 3, 021008 (2013).
- [13] G. de Lange, D. Risté, M. J. Tiggelman, C. Eichler, L. Tornberg, G. Johansson, A. Wallraff, R. N. Schouten, and L. Dicarlo, Reversing Quantum Trajectories with Analog Feedback, *Phys. Rev. Lett.* 112, 080501 (2014).
- [14] Y. Masuyama, K. Funo, Y. Murashita, A. Noguchi, S. Kono, Y. Tabuchi, R. Yamazaki, M. Ueda, and Y. Nakamura, Information-to-Work Conversion by Maxwell's Demon in a Superconducting Circuit Quantum Electrodynamical System, *Nat. Commun.* 9, 4 (2018).
- [15] Y. Salathé, P. Kurpiers, T. Karg, C. Lang, C. K. Andersen, A. Akin, S. Krinner, C. Eichler, and A. Wallraff, Low-Latency Digital Signal Processing for Feedback and Feedforward in Quantum Computing and Communication, *Phys. Rev. Appl.* 9, 034011 (2018).
- [16] L. Hu, Y. Ma, W. Cai, X. Mu, Y. Xu, W. Wang, Y. Wu, H. Wang, Y. P. Song, C. L. Zou, S. M. Girvin, L. M. Duan, and L. Sun, Quantum Error Correction and Universal Gate Set Operation on a Binomial Bosonic Logical Qubit, *Nat. Phys.* 15, 503 (2019).
- [17] C. K. Andersen, A. Remm, S. Lazar, S. Krinner, J. Heinsoo, M. Gabureac, A. Wallraff, and C. Eichler, Entanglement Stabilization Using Ancilla-Based Parity Detection and Real-Time

- Feedback in Superconducting Circuits, *Npj Quantum Inf.* 5, 1 (2019).
- [18] R. Barends, J. Kelly, A. Megrant, A. Veitia, D. Sank, E. Jeffrey, T. C. White, J. Mutus, A. G. Fowler, B. Campbell, Y. Chen, Z. Chen, B. Chiaro, A. Dunsworth, C. Neill, P. J. J. O'Malley, P. Roushan, A. Vainsencher, J. Wenner, A. N. Korotkov, A. N. Cleland, and J. M. Martinis, Superconducting Quantum Circuits at the Surface Code Threshold for Fault Tolerance, *Nature* 508, 500 (2014).
- [19] J. Kelly, R. Barends, A. G. Fowler, A. Megrant, E. Jeffrey, T. C. White, D. Sank, J. Y. Mutus, B. Campbell, Y. Chen, Z. Chen, B. Chiaro, A. Dunsworth, I. C. Hoi, C. Neill, P. J. J. O'Malley, C. Quintana, P. Roushan, A. Vainsencher, J. Wenner, A. N. Cleland, and J. M. Martinis, State Preservation by Repetitive Error Detection in a Superconducting Quantum Circuit, *Nature* 519, 66 (2015).
- [20] X. Fu, M. A. Rol, C. C. Bultink, J. Van Someren, N. Khammassi, I. Ashraf, R. F. L. Vermeulen, J. C. De Sterke, W. J. Vlothuizen, R. N. Schouten, C. G. Almudver, L. DiCarlo, and K. Bertels, An Experimental Microarchitecture for a Superconducting Quantum Processor, *Proc. 50th Annu. IEEE/ACM Int. Symp. Microarchitecture - MICRO-50* 17 813 (2017).
- [21] J. M. Gambetta, J. M. Chow, and M. Steffen, Building Logical Qubits in a Superconducting Quantum Computing System, *Npj Quantum Inf.* 3, 0 (2017).
- [22] M. D. Reed, B. R. Johnson, A. A. Houck, L. Dicarlo, J. M. Chow, D. I. Schuster, L. Frunzio, and R. J. Schoelkopf, Fast Reset and Suppressing Spontaneous Emission of a Superconducting Qubit, *Appl. Phys. Lett.* 96, 203110 (2010).
- [23] E. Jeffrey, D. Sank, J. Y. Mutus, T. C. White, J. Kelly, R. Barends, Y. Chen, Z. Chen, B. Chiaro, A. Dunsworth, A. Megrant, P. J. J. O'Malley, C. Neill, P. Roushan, A. Vainsencher, J. Wenner, A. N. Cleland, and J. M. Martinis, Fast Accurate State Measurement with Superconducting Qubits, *Phys. Rev. Lett.* 112, 190504 (2014).
- [24] Z. Zhang, T. Wang, L. Xiang, Z. Jia, P. Duan, W. Cai, Z. Zhan, Z. Zong, J. Wu, L. Sun, Y. Yin and G. Guo, Experimental Demonstration of Work Fluctuations along a Shortcut to Adiabaticity with a Superconducting Xmon Qubit, *New J. Phys.* 20, 085001 (2018).
- [25] T. Wang, Z. Zhang, L. Xiang, Z. Jia, P. Duan, W. Cai, Z. Gong, Z. Zong, M. Wu, J. Wu, L. Sun, Y. Yin, and G. Guo, The Experimental Realization of High-Fidelity Shortcut-to-Adiabaticity Quantum Gates in a Superconducting Xmon Qubit, *New J. Phys.* 20, 065003 (2018).

- [26] T. Wang, Z. Zhang, L. Xiang, Z. Jia, P. Duan, Z. Zong, Z. Sun, Z. Dong, J. Wu, Y. Yin, and G. Guo, Experimental Realization of a Fast Controlled-Z Gate via a Shortcut to Adiabaticity, *Phys. Rev. Appl.* 11, 034030 (2019).
- [27] J. Koch, T. M. Yu, J. Gambetta, A. A. Houck, D. I. Schuster, J. Majer, A. Blais, M. H. Devoret, S. M. Girvin, and R. J. Schoelkopf, Charge-Insensitive Qubit Design Derived From the Cooper Pair Box, *Phys. Rev. A.* 76, 042319 (2007).
- [28] T. Roy, S. Kundu, M. Chand, A. M. Vadiraj, A. Ranadive, N. Nehra, M. P. Patankar, J. Aumentado, A. A. Clerk, and R. Vijay, Broadband Parametric Amplification with Impedance Engineering: Beyond the Gain-Bandwidth Product, *Appl. Phys. Lett.* 107, 262601 (2015).
- [29] F. Mallet, F. R. Ong, A. Palacios-Laloy, F. Nguyen, P. Bertet, D. Vion, and D. Esteve, Single-Shot Qubit Readout in Circuit Quantum Electrodynamics, *Nat. Phys.* 5, 791 (2009).
- [30] V. Negnevitsky, M. Marinelli, K. K. Mehta, H. Y. Lo, C. Flhmann, and J. P. Home, Repeated Multi-Qubit Readout and Feedback with a Mixed-Species Trapped-Ion Register, *Nature* 563, 527 (2018).
- [31] M. Steffen, M. Ansmann, R. Mcdermott, N. Katz, R. C. Bialczak, E. Lucero, M. Neeley, E. M. Weig, A. N. Cleland, and J. M. Martinis, State Tomography of Capacitively Shunted Phase Qubits with High Fidelity, *Phys. Rev. Lett.* 97, 050502 (2006).